

Importance of higher harmonics and v_4 puzzle in quark-gluon plasma tomography

Dusan Zigic, Jussi Auvinen, Igor Salom, and Magdalena Djordjevic*

Institute of Physics Belgrade, University of Belgrade, Serbia

Pasi Huovinen

Institute of Physics Belgrade, University of Belgrade, Serbia and

Incubator of Scientific Excellence—Centre for Simulations

of Superdense Fluids, University of Wroclaw, Poland

QGP tomography aims to constrain the parameters characterizing the properties and evolution of Quark-Gluon Plasma (QGP) formed in heavy-ion collisions, by exploiting low and high- p_\perp theory and data. Higher-order harmonics v_n ($n > 2$) are an important—but seldom explored—part of this approach. However, to take full advantage of them, several issues have to be addressed: i) consistency of different methods for calculating v_n , ii) importance of event-by-event fluctuations to high- p_\perp R_{AA} and v_2 predictions, iii) sensitivity of higher harmonics to the initial state of fluid-dynamical evolution. We obtain that i) several methods for calculating harmonics are compatible with each other, ii) event-by-event calculations are important in mid-central collisions, and iii) various initializations of the evolution of the medium lead to quantitatively and qualitatively different predictions, likely to be distinguished by future measurements. We also find that the present high- p_\perp v_4 data cannot be reproduced using initial states for fluid-dynamical evolution given by state-of-the-art models. We call this discrepancy high- p_\perp v_4 puzzle at the LHC.

I. INTRODUCTION

During the past two decades, an impressive experimental and theoretical effort has been invested in generating and exploring a new form of matter called Quark-Gluon Plasma (QGP) [1–4]. This form of matter consists of interacting and no longer confined quarks, antiquarks, and

* E-mail: magda@ipb.ac.rs

gluons [5, 6] and is created at extremely high energy densities achieved in ultra-relativistic heavy ion collisions at the Relativistic Heavy Ion Collider (RHIC) and the Large Hadron Collider (LHC) experiments. An unprecedented amount of data for different collision systems (large and small), collision energies, types of particles, momentum regions, centralities, etc., are generated in these experiments, and one of the major current goals is to optimally use these data to investigate the properties of this exciting form of matter.

As one of the latest experimental achievements, the high momentum (high- p_{\perp}) higher harmonics have recently become available at RHIC and the LHC. For example, for charged hadrons, the data are available up to the 7th harmonic (for ATLAS [7]) and cover the p_{\perp} region up to 100 GeV (for CMS [8]). For heavy flavor, the coverage is not that extensive (for both harmonics and momentum region)—still, the upcoming experimental data at high-luminosity LHC Run3 should provide these data for both light and heavy flavor with much higher precision. In the upcoming RHIC (sPHENIX and STAR) experiments, similar quality data is expected, with p_{\perp} coverage up to 20 GeV. Even if the p_{\perp} range accessible at RHIC is narrower than at the LHC, it is particularly useful for QGP tomography due to the pronounced difference between light and heavy flavor in that region. While these data (will) represent the state-of-the-art in the experimental sector, theoretically the higher harmonics at high- p_{\perp} have not been well explored.

To use these data for QGP tomography, i.e., for exploring the bulk QGP properties through high- p_{\perp} theory and data, one should first identify and address potential limitations, in particular related to coverage and design of different experiments. For example, four different methods are commonly used in the literature to evaluate v_n : two-particle cumulant $v_n\{2\}$, four-particle cumulant $v_n\{4\}$, event plane $v_n\{EP\}$, and scalar product $v_n\{SP\}$ methods (see section II C for more details). Do these methods provide consistent results, especially when different experimental collaborations even define $v_n\{SP\}$ in different ways?

Furthermore, in experimental analysis, the scalar product method correlates the particle of interest at midrapidity with the bulk medium constituents at higher rapidity regions to avoid non-flow effects on measured v_n [7, 8]. From theoretical perspective, this means the use of the experimental definition for $v_n\{SP\}$ necessitates 3+1D hydrodynamic modeling for event-by-event simulations. However, 3+1D simulations are computationally several orders of magnitude more demanding than 2+1D simulations and consequently time-wise impractical for high precision QGP tomography. Thus, the question arises whether it would be plausible to compare $v_n\{SP\}$ obtained in boost-invariant 2+1D simulations to experimental data in a model where the high-

and low- p_{\perp} particles have separate sources (fragmenting jets and a thermal fireball, respectively), and are thus uncorrelated.

Next, for the second harmonic, v_2 , event-by-event fluctuations are expected to either have a significant effect on v_2 values [9], or to be small enough to be considered negligible [10, 11]. However, these studies were done in limited and different centrality regions. It is expected [12] that the effects of event-by-event fluctuations increase with decreasing centrality. Thus, it is important to systematically investigate and quantify these effects for the high- p_{\perp} region at different centralities.

Therefore, the study presented in this manuscript has the following main goals:

- (i) Explore to what extent the different methods for calculating higher harmonics are compatible with each other.
- (ii) Explore the importance of event-by-event fluctuations and correlations to high- p_{\perp} v_2 and R_{AA} .
- (iii) Explore the qualitative and quantitative effects of different medium evolution scenarios on high- p_{\perp} higher harmonics, and how well the existing high- p_{\perp} data can be reproduced without further tuning of parameters.

Overall, this study explores whether and how high- p_{\perp} higher harmonics, with an adequate theoretical framework, can provide further constraints to the bulk QGP properties.

II. METHODS

A. Outline of DREENA-A framework

To use the high- p_{\perp} particles to explore the bulk properties, we developed a fully optimized modular framework DREENA-A [13], where ‘‘DREENA’’ stands for Dynamical Radiative and Elastic ENergy loss Approach, while ‘‘A’’ stands for Adaptive. We further optimized the framework for this study to efficiently incorporate any, arbitrary, event-by-event fluctuating temperature profile within the dynamical energy loss formalism. Due to the very large amount of temperature profile data processed in event-by-event calculations, we optimized file handling and formats. Also, we reorganized the parallelization of computation, as well as ensured that spatio-

temporal resolution and calculation precision are optimal and adjusted to the event-by-event type of profiles.

The framework does not have fitting parameters within the energy loss model (i.e., all parameters used in the model correspond to standard literature values), which allows to systematically compare the data and predictions obtained by the same formalism and parameter set. Therefore different temperature profiles (which are the only input in the DREENA-A framework) resulting from different initial states, and QGP properties, can be distinguished by the high- p_{\perp} observables they lead to, and the bulk QGP properties can be further constrained by studying low and high- p_{\perp} theory and data jointly.

The dynamical energy loss formalism [14–16] has several important features, all of which are needed for accurate predictions [17]: *i)* QCD medium of *finite* size and temperature consisting of dynamical (i.e., moving) partons. *ii)* Calculations are based on generalized Hard-Thermal-Loop approach [18], with naturally regulated infrared divergences [14, 16, 19]. *iii)* Both radiative [14, 15] and collisional [16] energy losses are calculated in the same theoretical framework and apply to both light and heavy flavors. *iv)* The framework is generalized toward running coupling [20] and finite magnetic mass [21]. We have also investigated the validity of the widely used soft-gluon approximation [22], but found it a very good approximation which does not need to be relaxed.

The initial quark spectrum, for light and heavy partons, is computed at next to leading order [23]. We use DSS [24] fragmentation functions to generate charged hadrons, and BCFY [25] and KLP [26] fragmentation functions for D and B mesons, respectively. To generate high- p_{\perp} predictions, we use the same parameter set as in DREENA-A [13]. Specifically, we assume effective light quark flavors $n_f = 3$ and $\Lambda_{QCD} = 0.2$ GeV. The temperature-dependent Debye mass μ_E is obtained by applying the procedure from [27] and leads to results compatible with the lattice QCD [28]. For the gluon mass, we assume $m_g = \mu_E/\sqrt{2}$ [19], and for light quark mass $M = \mu_E/\sqrt{6}$. The charm mass is $M = 1.2$ GeV and the bottom mass is $M = 4.75$ GeV. For magnetic to electric mass ratio, we use $\mu_M/\mu_E = 0.5$ [29, 30].

B. Modeling the bulk evolution

We investigate three different event-by-event initializations for the bulk evolution. The first is Monte Carlo Glauber (MC-Glauber) initialization at initial time $\tau_0 = 1.0$ fm without initial transverse flow. We assign the binary collision points at halfway between the two colliding

nucleons and convert these points to a continuous binary collision density using 2-D Gaussian distributions

$$n_{BC}(x, y) = \frac{1}{2\pi\sigma_{BC}^2} \sum_{i=1}^{N_{BC}} \exp\left(-\frac{(x-x_i)^2 + (y-y_i)^2}{2\sigma_{BC}^2}\right) \quad (1)$$

with a width parameter $\sigma_{BC} = 0.35$ fm. The binary collision density is then converted to energy density with the formula

$$\epsilon(x, y) = C_0(n_{BC} + c_1 n_{BC}^2 + c_2 n_{BC}^3), \quad (2)$$

and further extended in the longitudinal direction using the LHC parametrization from Ref. [31]. The evolution of the fluid is calculated using a 3+1D viscous fluid code [31], with a constant shear viscosity over entropy density ratio $\eta/s = 0.03$ and no bulk viscosity. The equation of state (EoS) parametrization is *s95p*-PCE-v1 [32]. The model parameters were tuned to ALICE charged particle multiplicity [33] and $v_n(p_\perp)$ data [34] for 10-20%, 20-30% and 30-40% centrality classes in Pb+Pb collisions at $\sqrt{s_{NN}} = 5.02$ TeV.

The second model is the T_RENTo initialization [35] with a free streaming stage until $\tau_0 = 1.16$ fm, further evolved using the VISH2+1 code [36] as described in [37, 38]. The parameters in this calculation are based on a Bayesian analysis of the data at Pb+Pb collisions at $\sqrt{s_{NN}} = 2.76$ and 5.02 TeV [38]. In particular the calculation includes temperature dependent shear and bulk viscosity coefficients with the minimum value of $\eta/s = 0.081$ and maximum of $\zeta/s = 0.052$. The EoS [37] is based on the lattice results by the HotQCD collaboration [39].

The third investigated initialization model is IP-Glasma [40, 41]. The calculated event-by-event fluctuating initial states [42] are further evolved [43] using the MUSIC code [44–46] constrained to boost-invariant expansion. In these calculations, the switch from Yang-Mills to fluid-dynamical evolution takes place at $\tau_{\text{switch}} = 0.4$ fm, shear viscosity over entropy density ratio is constant $\eta/s = 0.12$, and the temperature-dependent bulk viscosity coefficient over entropy density ratio has the maximum value $\zeta/s = 0.13$. The equation of state is based on the HotQCD lattice results [39] as presented in Ref. [47].

C. Flow analysis

1. Scalar product and event plane methods

We start by defining the low- p_\perp normalized flow vector for n -th harmonic based on M particles as

$$Q_n = \frac{1}{M} \sum_{j=1}^M e^{in\phi_j} \equiv |v_n| e^{in\Psi_n}, \quad (3)$$

where Ψ_n is the event plane angle: $\Psi_n = \arctan(\frac{\text{Im} Q_n}{\text{Re} Q_n})/n$.

Similarly to low p_\perp , we can define the flow vector for a high p_\perp bin as $(R_{AA}(p_\perp) = \frac{1}{2\pi} \int_0^{2\pi} R_{AA}(p_\perp, \phi) d\phi)$

$$q_n^{\text{hard}} = \frac{\frac{1}{2\pi} \int_0^{2\pi} e^{in\phi} R_{AA}(p_\perp, \phi) d\phi}{R_{AA}(p_\perp)}, \quad (4)$$

and single-event high- p_\perp flow coefficients v_n^{hard} as [9]

$$v_n^{\text{hard}} = \frac{\frac{1}{2\pi} \int_0^{2\pi} \cos[n(\phi - \Psi_n^{\text{hard}}(p_\perp))] R_{AA}(p_\perp, \phi) d\phi}{R_{AA}(p_\perp)} \quad (5)$$

where the event plane angle $\Psi_n^{\text{hard}}(p_\perp)$ is defined as

$$\Psi_n^{\text{hard}}(p_\perp) = \frac{1}{n} \arctan \left(\frac{\int_0^{2\pi} \sin(n\phi) R_{AA}(p_\perp, \phi) d\phi}{\int_0^{2\pi} \cos(n\phi) R_{AA}(p_\perp, \phi) d\phi} \right). \quad (6)$$

The high- p_\perp v_n is then calculated by correlating q_n with Q_n [9, 10, 48]:

$$v_n^{\text{hard}}\{\text{SP}\} = \frac{\langle \text{Re}(q_n^{\text{hard}}(Q_n)^*) \rangle_{\text{ev}}}{\sqrt{\langle Q_n(Q_n)^* \rangle_{\text{ev}}}} = \frac{\langle |v_n^{\text{hard}}| |v_n| \cos[n(\Psi_n^{\text{hard}}(p_\perp) - \Psi_n)] \rangle_{\text{ev}}}{\sqrt{\langle |v_n|^2 \rangle_{\text{ev}}}}. \quad (7)$$

We may also simply calculate the high- p_\perp anisotropy with respect to the event plane Ψ_n , which we shall denote as the ‘‘event plane’’ v_n [10]:

$$v_n\{\text{EP}\} = \langle \langle \cos[n(\phi^{\text{hard}} - \Psi_n)] \rangle \rangle_{\text{ev}} = \langle v_n^{\text{hard}} \cos[n(\Psi_n^{\text{hard}} - \Psi_n)] \rangle_{\text{ev}}. \quad (8)$$

For our theoretical $v_n\{\text{SP}\}$, the reference flow vector Q_n is calculated using only midrapidity particles. In order to reduce non-flow effects, it is common in experiments to introduce a rapidity gap between the particles of interest and the reference flow particles. ATLAS defines the scalar product v_n as [7]:

$$v_n\{\text{SP}_{\text{ATLAS}}\} = \frac{\text{Re} \langle \langle e^{in\phi} (Q_n^{-|+})^* \rangle \rangle_{\text{ev}}}{\sqrt{\langle Q_n^- (Q_n^+)^* \rangle_{\text{ev}}}} \quad (9)$$

where $Q_n^- = \frac{1}{M^-} \sum_{j=1}^{M^-} e^{in\phi_j}$ refers to particles in the rapidity interval $-4.9 < \eta < -3.2$ and Q_n^+ similarly to particles in the interval $3.2 < \eta < 4.9$, while $e^{in\phi}$ is associated with particles in midrapidity $|\eta| < 2.5$. $Q_n^{-|+}$ indicates that particle of interest with $\eta < 0$ are coupled to Q_n^+ and particles with $\eta > 0$ to Q_n^- to maximize the rapidity gap¹.

CMS definition for the scalar product is [8]

$$v_n\{\text{SP}_{\text{CMS}}\} = \frac{\text{Re} \langle Q_n Q_{nA}^* \rangle_{\text{ev}}}{\sqrt{\frac{\langle Q_{nA} Q_{nB}^* \rangle_{\text{ev}} \langle Q_{nA} Q_{nC}^* \rangle_{\text{ev}}}{\langle Q_{nB} Q_{nC}^* \rangle_{\text{ev}}}}} \quad (10)$$

where the flow vector $Q_n = \sum_{j=1}^M e^{in\phi_j}$ consists of particles of interest in midrapidity $|\eta| < 1.0$, vectors $Q_{nA}, Q_{nB} = \sum_{j=1}^{M_{A,B}} E_T e^{in\phi_j}$ are measured from the HF calorimeters at $2.9 < |\eta| < 5.2$, one at the negative and the other at the positive rapidity, and the third reference vector $Q_{nC} = \sum_{j=1}^{M_C} p_\perp e^{in\phi_j}$ is obtained from tracks with $|\eta| < 0.75$. If the particle of interest comes from the positive- η side of the tracker, then Q_{nA} is calculated using the negative- η side of HF, and vice versa.

2. Cumulant method

For 2- and 4-particle cumulant analysis, we use the unnormalized flow vector:

$$\tilde{Q}_n = \sum_{j=1}^M e^{in\phi_j}. \quad (11)$$

The low- p_\perp integrated reference flow is calculated using Eqs. (7)-(18) from Ref. [49]: The 2-particle cumulant v_n is defined as

$$v_n\{2\} = \sqrt{c_n\{2\}}, \quad (12)$$

where the second order cumulant $c_n\{2\}$ equals the event-averaged 2-particle correlation $\langle\langle 2 \rangle\rangle_{\text{ev}}$.

The 4-particle cumulant v_n is

$$v_n\{4\} = \sqrt[4]{-c_n\{4\}}, \quad (13)$$

where $c_n\{4\}$ is the 4th order cumulant $\langle\langle 4 \rangle\rangle_{\text{ev}} - 2\langle\langle 2 \rangle\rangle_{\text{ev}}^2$.

For a single event, the 2-particle correlation is

$$\langle 2 \rangle = \frac{|\tilde{Q}_n|^2 - M}{W_2} \quad (14)$$

¹ Since our high- p_\perp particles are produced at $\eta = 0$, the choice of Q_n^+ or Q_n^- for the correlation is arbitrary.

with a combinatorial weight factor $W_2 = M(M - 1)$ and the single-event 4-particle correlation is

$$\langle 4 \rangle = \frac{|\tilde{Q}_n|^4 + |\tilde{Q}_{2n}|^2 - 2\text{Re}|\tilde{Q}_{2n}\tilde{Q}_n^*\tilde{Q}_n^*|}{W_4} - 2\frac{2(M-2)|\tilde{Q}_n|^2 - M(M-3)}{W_4} \quad (15)$$

with $W_4 = M(M - 1)(M - 2)(M - 3)$.

Using the weight factors defined above, the weighted average of a k -particle correlation over multiple events is then

$$\langle \langle k \rangle \rangle_{\text{ev}} = \frac{\sum_{i=1}^{N_{\text{events}}} W_{k,i} \langle k \rangle_i}{\sum_{i=1}^{N_{\text{events}}} W_{k,i}}. \quad (16)$$

Once the reference flow has been determined, the p_T -differential flow can be calculated using Eqs. (20)-(35) of [49]. Here we denote the flow vector in a p_\perp bin with m_q particles as

$$q_n = \sum_{j=1}^{m_q} e^{in\phi_j}. \quad (17)$$

For high- p_\perp particles, q_n is calculated from the distribution

$$q_n = \int_0^{2\pi} e^{in\phi} \frac{dN}{dp_\perp d\phi} d\phi \quad (18)$$

with the associated multiplicity

$$m_q = \int_0^{2\pi} \frac{dN}{dp_\perp d\phi} d\phi. \quad (19)$$

For high- p_\perp differential flow, none of the particles in a p_\perp bin are included in the calculation of the reference flow, so the weight factors are $W'_2 = m_q M$ and $W'_4 = m_q M(M - 1)(M - 2)$, and the 2-particle correlation is simply

$$\langle 2' \rangle = \frac{q_n \tilde{Q}_n^*}{W'_2}, \quad (20)$$

while the 4-particle correlation is

$$\langle 4' \rangle = \frac{q_n \tilde{Q}_n \tilde{Q}_n^* \tilde{Q}_n^* - q_n \tilde{Q}_n \tilde{Q}_{2n}^* - 2M q_n \tilde{Q}_n^* + 2q_n \tilde{Q}_n^*}{W'_4}. \quad (21)$$

With the knowledge of the correlations, we can calculate the differential cumulants

$$\begin{aligned} d_n \{2\} &= \langle \langle 2' \rangle \rangle_{\text{ev}}, \\ d_n \{4\} &= \langle \langle 4' \rangle \rangle_{\text{ev}} - 2 \langle \langle 2' \rangle \rangle_{\text{ev}} \langle \langle 2' \rangle \rangle_{\text{ev}} \end{aligned} \quad (22)$$

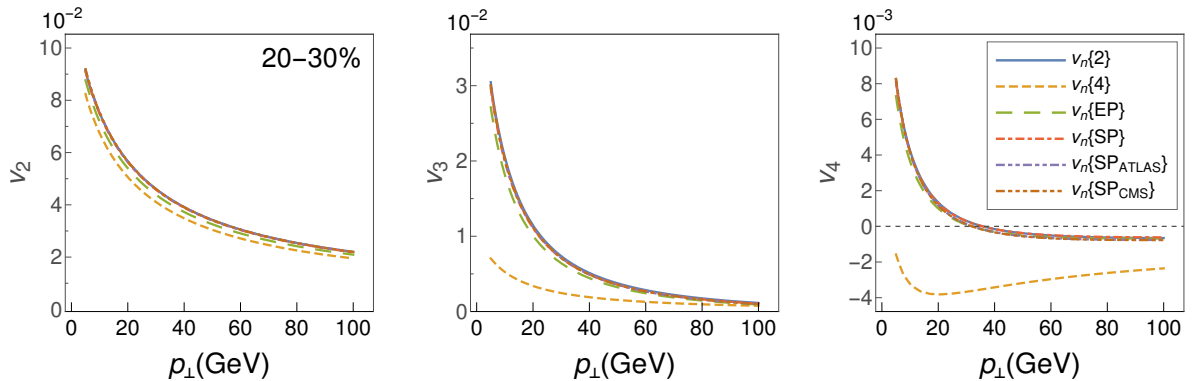


FIG. 1: Charged hadron v_2 (left), v_3 (middle) and v_4 (right) in Pb+Pb collisions at $\sqrt{s_{\text{NN}}} = 5.02$ TeV for 20-30% centrality class, computed using different analysis methods: 2-particle cumulant, 4-particle cumulant, event plane, midrapidity scalar product, ATLAS-defined scalar product, and CMS defined scalar product, each described in the section II C. Energy loss calculation was performed on MC-Glauber+3d-hydro temperature profiles, with $\mu_M/\mu_E = 0.5$.

and the differential flow

$$\begin{aligned}
 v'_n\{2\} &= \frac{d_n\{2\}}{\sqrt{c_n\{2\}}}, \\
 v'_n\{4\} &= -\frac{d_n\{4\}}{(-c_n\{4\})^{3/4}}.
 \end{aligned}
 \tag{23}$$

III. RESULTS AND DISCUSSION

A. Compatibility of analysis methods

In Fig. 1, we compare $v_n(p_\perp)$ for high- p_\perp particles obtained using six different methods: 2-particle cumulant $v_n\{2\}$ given by Eq. (12), 4-particle cumulant $v_n\{4\}$ given by Eq. (13), event plane $v_n\{\text{EP}\}$ defined by Eq. (8), midrapidity scalar product $v_n\{\text{SP}\}$ calculated using Eq. (7), scalar product $v_n\{\text{SP}_{\text{ATLAS}}\}$ as defined by the ATLAS collaboration (Eq. (9)), and scalar product $v_n\{\text{SP}_{\text{CMS}}\}$ as defined by the CMS collaboration (Eq. (10)). High- p_\perp R_{AA} and v_n predictions were obtained using generalized DREENA-A framework with the temperature profiles calculated using the combination of 3+1D viscous fluid code and MC-Glauber initial conditions (i.e., the first bulk model described in the section II B).

As illustrated in Fig. 1, different scalar product methods for evaluating the v_n coefficients, and the 2-particle cumulant method, lead to the same results with $\approx 5\%$ level accuracy. In agreement

with Refs. [10, 11, 50], the event plane results are also comparable to the scalar product results deviating only $\approx 10\%$, i.e., less than the current experimental uncertainty. The only method with significantly different results is the four-particle cumulant method $v_n\{4\}$, which is expected to differ from $v_n\{2\}$ in the presence of event-by-event fluctuations [12, 51]. The equivalence of different approaches simplifies comparison between theoretical predictions and experimental results, since a theoretical prediction calculated using any method (with the exception of the 4-particle cumulant method) can be directly compared to experimental data analyzed using any method. We have also checked that, in the scalar product method, the rapidity of particles used to calculate the reference flow vector has a negligible impact on high- p_\perp particle v_n in our framework and setup, allowing us to make meaningful $v_n\{\text{SP}\}$ data comparisons using the boost-invariant hydro simulations. However, it must be remembered that the scalar product method with large rapidity gap can be affected by the event plane decorrelation at different rapidities [52, 53]. In our approach the event plane is the same independent of rapidity, and thus the effect of decorrelation is not included. How the event plane depends on rapidity depends on the model used to create the longitudinal structure of the initial state, and since there are very few theoretical constraints for it, we leave these studies for a later work.

B. Event-by-event fluctuations

To investigate the influence of event-by-event fluctuations on high- p_\perp observables, MC-Glauber initial conditions for all events within a single centrality class were averaged (we kept reaction planes aligned, and averaged binary collision densities before converting to energy density, (Eq. 2)) and then evolved using the 3+1D viscous fluid code (in a single run, instead of one run for each event). Obtained smooth temperature profile was used to calculate high- p_\perp predictions, and R_{AA} as well as $v_2\{2\}$ and $v_2\{4\}$ results were compared to those obtained using full event-by-event calculations (evolved separately for each event), see Fig 2.

We see that event-by-event fluctuations increase both R_{AA} and v_2 . While the effect on the R_{AA} values is rather small ($\approx 7\%$) and does not have clear centrality dependence, the effect on $v_2\{2\}$ is more pronounced and increases with decreasing centrality. Quantitatively, we obtain that the average difference between event-by-event $v_2\{2\}$ and $v_2\{2\}$ calculated using smooth temperature profile goes from 14% for the 40-50% centrality class to 32% in the 10-20% centrality class. The observed centrality dependence can be explained by the fact that with the increase in centrality,

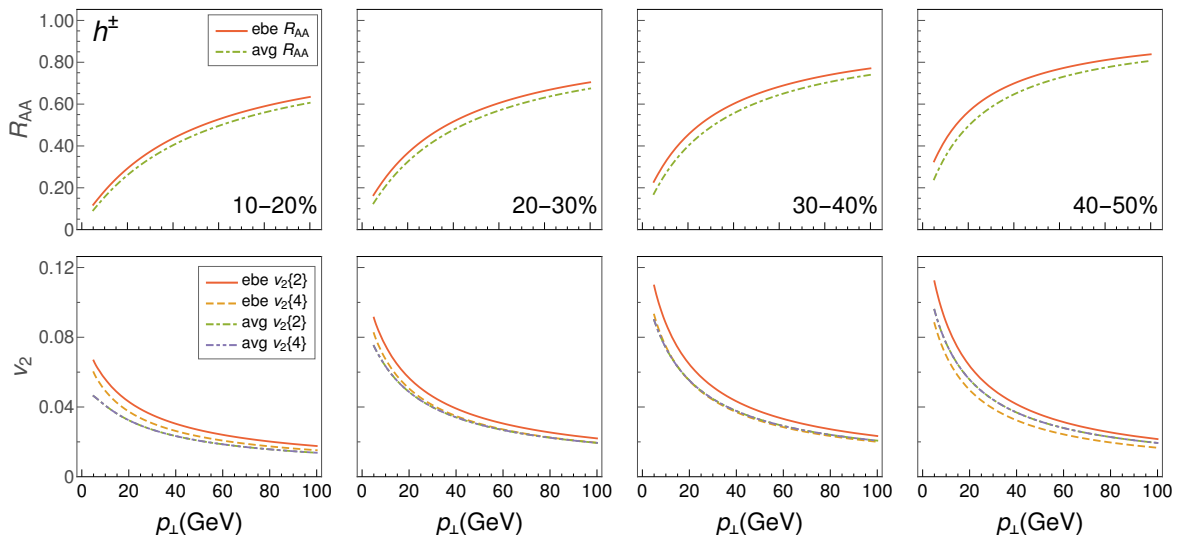


FIG. 2: *Upper panels:* charged hadron R_{AA} calculated using event-by-event (ebe) fluctuating temperature profiles compared to R_{AA} calculated using a smooth temperature profile (avg). *Lower panels:* charged hadron $v_n\{2\}$ and $v_n\{4\}$ calculated using event-by-event (ebe) fluctuating temperature profiles compared to $v_n\{2\}$ and $v_n\{4\}$ calculated using a smooth temperature profile (avg). Calculation was done for Pb+Pb collisions at $\sqrt{s_{NN}} = 5.02$ TeV, $\mu_M/\mu_E = 0.5$, using MC-Glauber+3d-hydro bulk evolution. Each column represents different centrality class (from left to right: 10-20%, 20-30%, 30-40% and 40-50%).

the influence of geometry on $v_2\{2\}$ becomes larger, while at low centralities, event-by-event fluctuations have the dominant impact on $v_2\{2\}$. We also observe a p_\perp dependence of these differences (generally decreasing with increasing p_\perp) and no notable difference between $v_2\{2\}$ and $v_2\{4\}$ when calculated on the smooth temperature profile, where initial state eccentricity fluctuations are absent.

C. Effects of initial state

To demonstrate the applicability of high- p_\perp theoretical predictions as a QGP tomography tool, we generated three different sets of temperature profiles using three different initial conditions and hydrodynamics codes. Generalized DREENA-A [13] was then used to calculate high- p_\perp predictions, which are compared to experimental data and, for charged hadrons, presented in Fig. 3, and for D and B mesons in Fig. 4. As can be seen, different initializations of fluid-dynamical evolution lead to different high- p_\perp predictions for both R_{AA} and v_2 , v_3 and v_4 , even

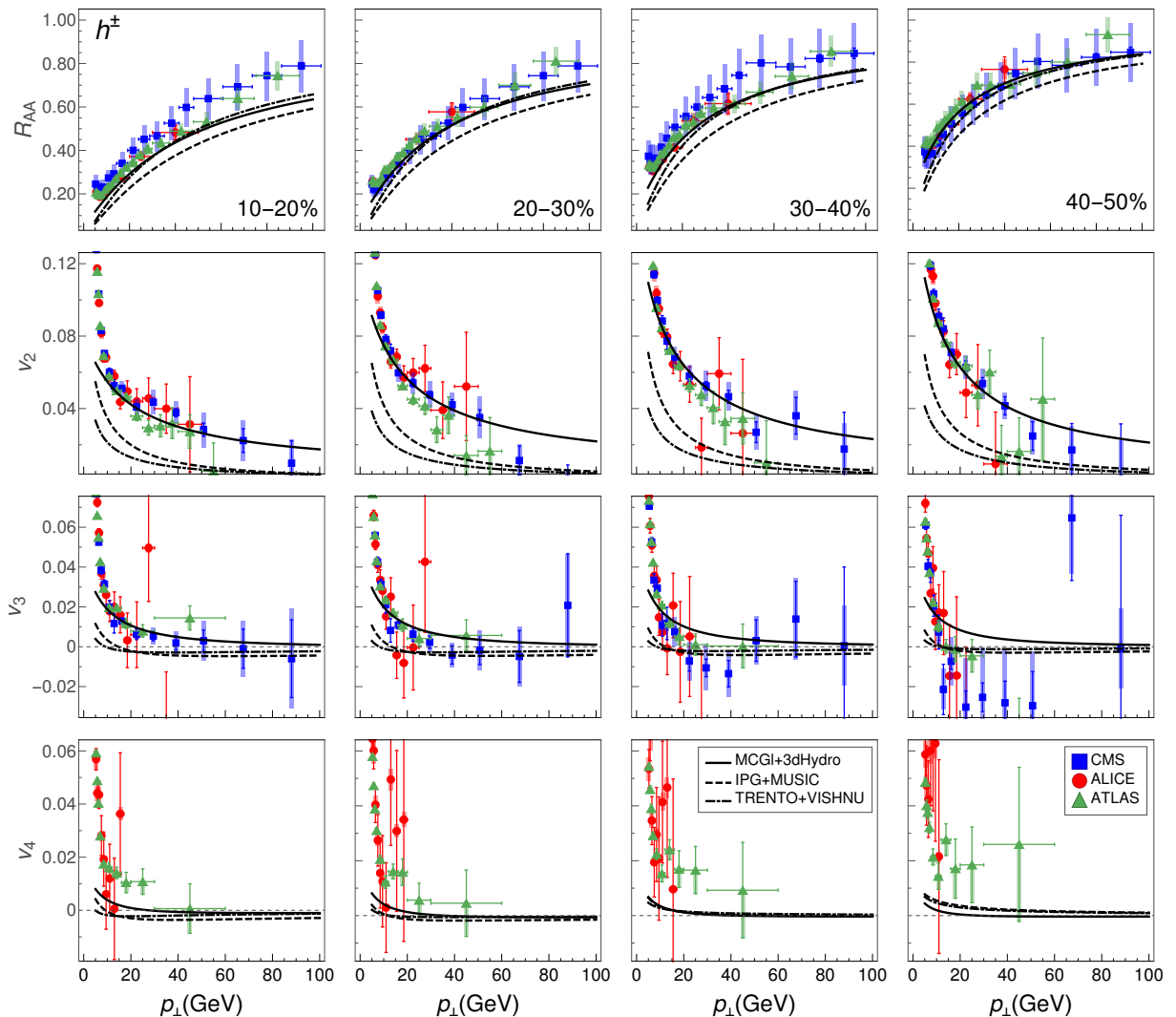


FIG. 3: Charged hadron R_{AA} (first row) v_2 (second row), v_3 (third row) and v_4 (fourth row) in Pb+Pb collisions at $\sqrt{s_{NN}} = 5.02$ TeV for different initializations of the QGP evolution (indicated in the legend). Theoretical predictions, obtained using SP method, are compared to CMS [8, 54] (blue squares), ALICE [55, 56] (red circles) and ATLAS [7, 57] (green triangles) data. Columns 1-4 correspond to, respectively, 10-20%, 20-30%, 30-40% and 40-50% centrality classes. $\mu_M/\mu_E = 0.5$.

though they all provide good agreement with low- p_{\perp} data. Specific differences are visible already on the level of R_{AA} values, where the IP-Glasma model results in discernibly stronger suppression. The differences in predictions become even higher when we consider the v_2 observable, with T_RENTo leading to lower v_2 than IP-Glasma, while MC-Glauber predictions are far above the two. A similar magnitude of relative differences is also obtained for v_3 and v_4 predictions, with an additional qualitative signature appearing for these observables: we notice that some

initializations lead to negative values of high- p_{\perp} v_3 and v_4 , i.e., models can differ even in the expected sign of the flow coefficients.

Since DREENA-A does not have fitting parameters in the energy loss (the only inputs are the temperature profile and binary collisions, which come as a direct output from fluid-dynamical calculation and the initial state model), Figs. 3 and 4 demonstrate that high- p_{\perp} R_{AA} and higher harmonics can distinguish between different initializations and temperature profiles, and subsequently further constrain their parameters. Furthermore, Fig. 4 suggests that heavy flavor high- p_{\perp} observables are even more sensitive to different temperature profiles than the light flavor. We also see that predictions for high- p_{\perp} higher harmonics can be either positive or negative. Thus, the high- p_{\perp} sector can provide both quantitative and qualitative constraints for different initial states.

Presently, of the considered models, the best agreement is observed for MC-Glauber. This result is compatible with our earlier findings [63], where the best agreement with high- p_{\perp} data was found by delaying the start of transverse expansion and energy loss to time $\tau_0 \approx 1.0$ fm. However, all models seem to vastly underestimate the v_4 values, though the error bars for the available v_4 data are quite large. If this tendency is preserved in future high luminosity experiments (e.g., in LHC run 3), it will present a new “high- p_{\perp} v_4 puzzle”, whose solution will require modifications to the present initial state models and/or energy loss mechanisms. Additionally, better quality heavy flavor data are needed, especially D and B-meson data, as they present valuable constraint to the evolution of the medium.

IV. SUMMARY

We obtained four main conclusions in this work: *i)* We found that different methods to calculate higher harmonics at high- p_{\perp} are compatible with each other within ≈ 5 –10% accuracy, which is less than the current experimental uncertainties. *ii)* Event-by-event calculations are particularly important for high- p_{\perp} v_2 in mid-central collisions. *iii)* Predictions for high- p_{\perp} observables, and especially for higher harmonics, are sensitive to the initial state of fluid-dynamical evolution, and can distinguish between different initial state models. *iv)* All initial state models lead to way smaller high- p_{\perp} v_4 than experimentally observed, and this disparity deserves to be called a “ v_4 puzzle”. Overall, the higher harmonics provide an exciting opportunity to obtain further constraints to the QGP properties and its evolution in heavy-ion collisions by combining new

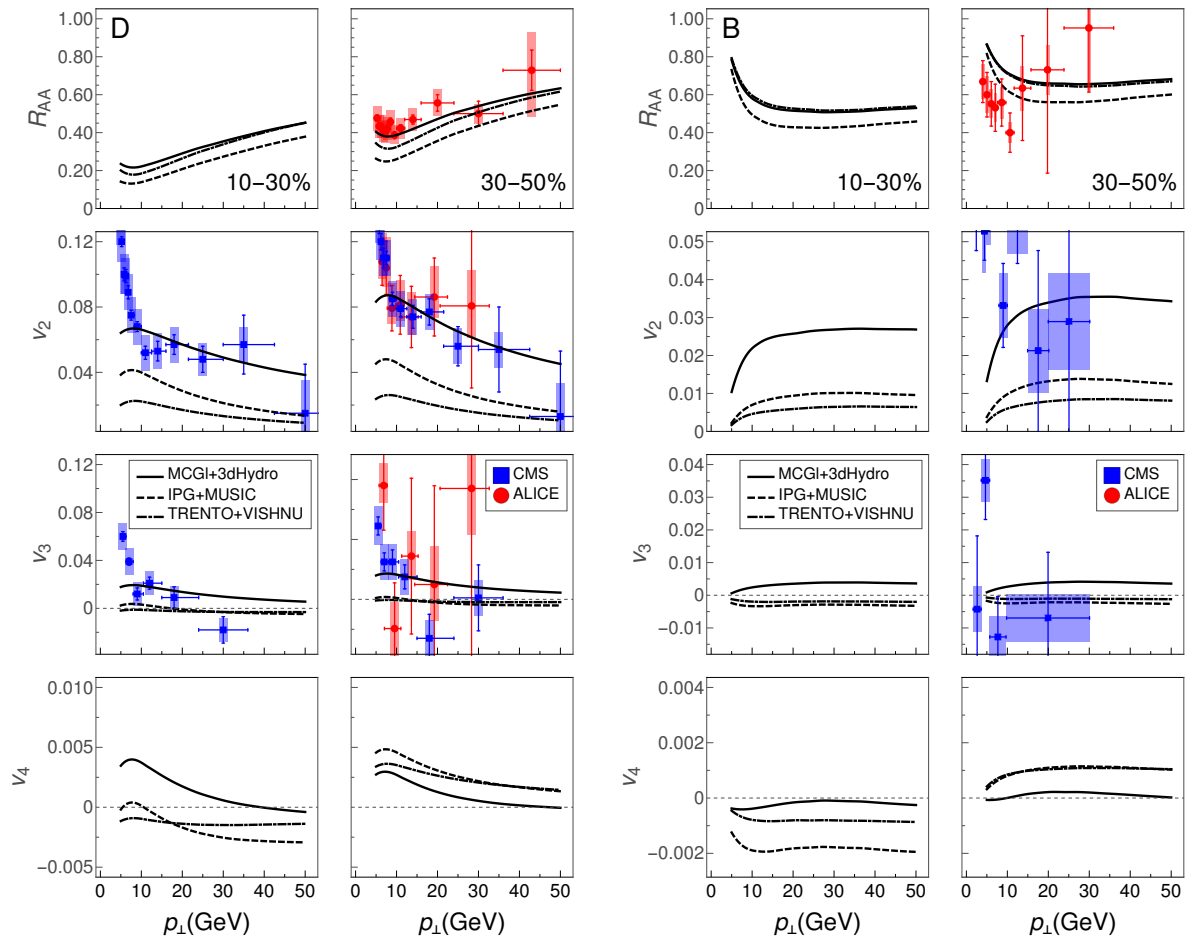


FIG. 4: D meson (left 4×2 panel) and B meson (right 4×2 panel) predictions in Pb+Pb collisions at $\sqrt{s_{NN}} = 5.02$ TeV for different initializations of QGP evolution (indicated in the legend). In each 4×2 panel, first row corresponds to R_{AA} , the second, third, fourth to v_2 , v_3 , v_4 , respectively, while the left (right) column corresponds to 10-30% (30-50%) centrality class. D meson theoretical predictions are compared to CMS [58] (blue squares) and ALICE [59, 60] (red circles) data, while B meson predictions are compared to preliminary CMS [61] (blue squares) and preliminary ALICE [62] (red circles) data for non-prompt D meson from b decay. $\mu_M/\mu_E = 0.5$.

theoretical developments (with the corresponding predictions) and upcoming higher luminosity experimental measurements.

Acknowledgments: We thank Chun Shen for sharing his results with us. We thank Marko Djordjevic, Bojana Ilic and Stefan Stojku for useful discussions. This work is supported by the European Research Council, grant ERC-2016-COG: 725741, and by the Ministry of Science

and Technological Development of the Republic of Serbia. PH was also supported by the program Excellence Initiative–Research University of the University of Wrocław of the Ministry of Education and Science.

-
- [1] E. V. Shuryak, Nucl. Phys. A **750**, 64 (2005); Rev. Mod. Phys. **89**, 035001 (2017).
 - [2] M. Gyulassy and L. McLerran, Nucl. Phys. A **750**, 30 (2005).
 - [3] B. Jacak and P. Steinberg, Phys. Today **63**, 39 (2010).
 - [4] B. Muller, J. Schukraft and B. Wyslouch, Ann. Rev. Nucl. Part. Sci. **62**, 361 (2012).
 - [5] J. C. Collins and M. J. Perry, Phys. Rev. Lett. **34**, 1353 (1975).
 - [6] G. Baym and S. A. Chin, Phys. Lett. B **62**, 241 (1976).
 - [7] M. Aaboud, *et al.* [ATLAS], Eur. Phys. J. C **78**, 997 (2018).
 - [8] A. M. Sirunyan, *et al.* [CMS], Phys. Lett. B **776**, 195 (2018).
 - [9] J. Noronha-Hostler, B. Betz, J. Noronha and M. Gyulassy, Phys. Rev. Lett. **116**, 252301 (2016).
 - [10] Y. He, W. Chen, T. Luo, S. Cao, L. G. Pang and X. N. Wang, [arXiv:2201.08408 [hep-ph]].
 - [11] S. Shi, J. Liao and M. Gyulassy, Chin. Phys. C **43**, 044101 (2019).
 - [12] B. Betz, M. Gyulassy, M. Luzum, J. Noronha, J. Noronha-Hostler, I. Portillo and C. Ratti, Phys. Rev. C **95**, 044901 (2017).
 - [13] D. Zigic, I. Salom, J. Auvinen, P. Huovinen and M. Djordjevic, [arXiv:2110.01544 [nucl-th]].
 - [14] M. Djordjevic, Phys. Rev. C **80**, 064909 (2009).
 - [15] M. Djordjevic and U. Heinz, Phys. Rev. Lett. **101**, 022302 (2008).
 - [16] M. Djordjevic, Phys. Rev. C **74**, 064907 (2006).
 - [17] B. Blagojevic and M. Djordjevic, J. Phys. G **42**, 075105 (2015).
 - [18] J. I. Kapusta, *Finite-Temperature Field Theory* (Cambridge University Press, 1989).
 - [19] M. Djordjevic and M. Gyulassy, Phys. Rev. C **68**, 034914 (2003).
 - [20] M. Djordjevic and M. Djordjevic, Phys. Lett. B **734**, 286 (2014).
 - [21] M. Djordjevic, Phys. Lett. B **709**, 229 (2012).
 - [22] B. Blagojevic, M. Djordjevic and M. Djordjevic, Phys. Rev. C **99**, 024901 (2019).
 - [23] Z. B. Kang, I. Vitev and H. Xing, Phys. Lett. B **718**, 482 (2012); R. Sharma, I. Vitev and B.W. Zhang, Phys. Rev. C **80**, 054902 (2009).
 - [24] D. de Florian, R. Sassot and M. Stratmann, Phys. Rev. D **75**, 114010 (2007).

- [25] M. Cacciari, P. Nason, JHEP **0309**, 006 (2003), E. Braaten, K.-M. Cheung, S. Fleming and T. C. Yuan, Phys. Rev. D **51**, 4819 (1995).
- [26] V. G. Kartvelishvili, A.K. Likhoded, V.A. Petrov, Phys. Lett. B **78**, 615 (1978).
- [27] A. Peshier, hep-ph/0601119 (2006).
- [28] O. Kaczmarek, F. Karsch, F. Zantow and P. Petreczky, Phys. Rev. D **70**, 074505 (2004); O. Kaczmarek and F. Zantow, Phys. Rev. D **71**, 114510 (2005).
- [29] Yu. Maezawa *et al.* [WHOT-QCD Collaboration], Phys. Rev. D **81** 091501 (2010).
- [30] A. Nakamura, T. Saito and S. Sakai, Phys. Rev. D **69**, 014506 (2004).
- [31] E. Molnar, H. Holopainen, P. Huovinen and H. Niemi, Phys. Rev. C **90**, 044904 (2014).
- [32] P. Huovinen and P. Petreczky, Nucl. Phys. A **837**, 26-53 (2010).
- [33] J. Adam *et al.* [ALICE Collaboration], Phys. Rev. Lett. **116**, 222302 (2016).
- [34] J. Adam *et al.* [ALICE Collaboration], Phys. Rev. Lett. **116**, 132302 (2016).
- [35] J. S. Moreland, J. E. Bernhard and S. A. Bass, Phys. Rev. C **92**, 011901 (2015).
- [36] H. Song and U. W. Heinz, Phys. Rev. C **77**, 064901 (2008).
- [37] J. E. Bernhard, arXiv:1804.06469 [nucl-th].
- [38] J. E. Bernhard, J. S. Moreland and S. A. Bass, Nature Phys. **15**, no.11, 1113-1117 (2019).
- [39] A. Bazavov *et al.* [HotQCD], Phys. Rev. D **90**, 094503 (2014).
- [40] B. Schenke, P. Tribedy and R. Venugopalan, Phys. Rev. Lett. **108**, 252301 (2012).
- [41] B. Schenke, P. Tribedy and R. Venugopalan, Phys. Rev. C **86**, 034908 (2012).
- [42] B. Schenke, C. Shen and P. Tribedy, Phys. Rev. C **102**, 044905 (2020)
- [43] C. Shen, private communication (2020).
- [44] B. Schenke, S. Jeon and C. Gale, Phys. Rev. C **82**, 014903 (2010).
- [45] B. Schenke, S. Jeon and C. Gale, Phys. Rev. Lett. **106**, 042301 (2011).
- [46] B. Schenke, S. Jeon and C. Gale, Phys. Rev. C **85**, 024901 (2012).
- [47] J. S. Moreland and R. A. Soltz, Phys. Rev. C **93**, 044913 (2016).
- [48] C. Andres, N. Armesto, H. Niemi, R. Paatelainen and C. A. Salgado, Phys. Lett. B **803**, 135318 (2020).
- [49] A. Bilandzic, R. Snellings and S. Voloshin, Phys. Rev. C **83**, 044913 (2011).
- [50] J. F. Paquet, C. Shen, G. S. Denicol, M. Luzum, B. Schenke, S. Jeon and C. Gale, Phys. Rev. C **93**, 044906 (2016).
- [51] S. A. Voloshin, A. M. Poskanzer, A. Tang and G. Wang, Phys. Lett. B **659**, 537 (2008).

- [52] J. Jia and P. Huo, *Phys. Rev. C* **90**, 034905 (2014).
- [53] V. Khachatryan *et al.* [CMS], *Phys. Rev. C* **92**, 034911 (2015).
- [54] V. Khachatryan *et al.* [CMS], *JHEP* **04**, 039 (2017).
- [55] S. Acharya *et al.* [ALICE], *JHEP* **11**, 013 (2018).
- [56] S. Acharya *et al.* [ALICE], *JHEP* **07**, 103 (2018).
- [57] [ATLAS], ATLAS-CONF-2017-012.
- [58] A. M. Sirunyan *et al.* [CMS], *Phys. Lett. B* **816**, 136253 (2021).
- [59] S. Acharya *et al.* [ALICE], *JHEP* **01**, 174 (2022).
- [60] S. Acharya *et al.* [ALICE], *Phys. Lett. B* **813**, 136054 (2021).
- [61] contribution link: <https://indico.cern.ch/event/895086/contributions/4314625/>
- [62] contribution link: <https://indico.cern.ch/event/895086/contributions/4715758/>
- [63] S. Stojku, J. Auvinen, M. Djordjevic, P. Huovinen and M. Djordjevic, *Phys. Rev. C* **105**, L021901 (2022).